

# Ab initio study of shock compressed oxygen

Cong Wang<sup>1</sup> and Ping Zhang<sup>1,2,\*</sup>

<sup>1</sup>*LCP, Institute of Applied Physics and Computational Mathematics,  
P.O. Box 8009, Beijing 100088, People's Republic of China*

<sup>2</sup>*Center for Applied Physics and Technology, Peking University, Beijing 100871, People's Republic of China*  
(Dated: November 12, 2018)

Quantum molecular dynamic simulations are introduced to study the shock compressed oxygen. The principal Hugoniot points derived from the equation of state agree well with the available experimental data. With the increase of pressure, molecular dissociation is observed. Electron spin polarization determines the electronic structure of the system under low pressure, while it is suppressed around 30 ~ 50 GPa. Particularly, nonmetal-metal transition is taken into account, which also occurs at about 30 ~ 50 GPa. In addition, the optical properties of shock compressed oxygen are also discussed.

PACS numbers: 62.50.+p, 71.30.+h, 61.20.Ja

## I. INTRODUCTION

The study of pressure-induced transformations of materials in the shock compressed fluid state is of great interest in the last decade<sup>1</sup>. In particular, the homonuclear diatomic molecular systems such as hydrogen<sup>2,3</sup>, oxygen<sup>4,5,6,7</sup>, nitrogen<sup>8,9</sup>, and the halogens<sup>10,11</sup>, have been intensively studied with a variety of experimental techniques, and the measurements of Hugoniot have reached megabar range. On the theoretical side, Quantum molecular dynamic (QMD) and path-integral Monte Carlo (PIMC) simulations<sup>12,13,14</sup> have been introduced in the study of materials under extreme conditions. In spite of fact that these theoretical simulations in some cases already provided explanatory and predictive results, to date, however, many fundamental questions of these above-mentioned systems in the fluid state are still under intense discussion due to the profound behavior they display.

A knowledge of the properties of oxygen, in particular, the equation of state (EOS) and derived properties, such as the Hugoniot curve and  $(D, u)$  diagram, are important for shocks, detonations, biology, and fluids. Single or multiple shock-wave experiments have been performed on oxygen<sup>4,5</sup>, and principal Hugoniot are determined from the EOS data. The partial molecular dissociation and a two-component conductive fluid are indicated by the results. Theoretically, a classical repulsive pair potential was introduced to investigate the EOS of shock-compressed oxygen<sup>15</sup>, and the dissociation effect of oxygen at high pressure was partially taken into account by using a classical self-consistent fluid variational theory<sup>16</sup>. Due to the intrinsic approximations of these classical methods, however, a full quantum-mechanical description of the change in the electronic structure of oxygen under high-pressure and high-temperature shock-wave compression still remains to be presented and understood. The necessity for such quantum-mechanical treatment of shock compressed oxygen can, for example, be clearly seen by the following facts: (i) QMD method, where the electrons are fully quantum mechan-

ical treated, has been proven successfully in calculating the electronic structure, thermodynamical and optical properties of warm dense matter<sup>17,18</sup>; (ii) nonmetal-metal transition of oxygen was observed recently<sup>6</sup>; (iii) low-pressure QMD calculations<sup>12</sup> already indicated importance of electron spin polarization effect during oxygen dissociation. From these facts, therefore, electronic structure should be seriously considered, the EOS data and Hugoniot points from density functional theory (DFT) are highly needed for shock compressed oxygen.

In the present work, we apply QMD simulations to study the thermophysical properties of shock compressed oxygen. We determine the EOS data and dissociation fraction of oxygen along the principal Hugoniot. The pair correlation function is derived from the structural information during QMD simulations. The electronic structure calculations within QMD provide the charge density in the simulation box and density of states (DOS) at every time step. The dissociation of oxygen and electronic structure are important for identifying nonmetal-metal transition. The dielectric function  $\epsilon(\omega)$  and the consequent optical quantities are also extracted.

## II. QUANTUM MOLECULAR DYNAMICS SIMULATIONS

In this study, we employ the VASP plane-wave pseudopotential code, which was developed at the Technical University of Vienna<sup>19,20</sup>. The finite temperature density functional theory molecular dynamics (FTDFT-MD)<sup>21,22</sup>, where the electronic states are populated according to a Fermi-Dirac distribution at temperature  $T_e$ , is used in the present work. The electron wave functions are calculated with the projector augmented wave (PAW) potential<sup>23,24</sup>. The exchange correlation functional is calculated within generalized gradient approximation (GGA) using the parametrization of Perdew-Wang 91<sup>25</sup>. Electron spin polarization, which can be effectively used to describe the character of O<sub>2</sub> molecules, is also considered in our calculation.

In all the simulations, a total number of 96 oxygen atoms (48 O<sub>2</sub> molecules) are included in a supercell with periodic boundary condition. Trajectories are calculated at separate densities and temperatures. The selected densities range from  $\rho=2.5$  to  $3.6$  g/cm<sup>3</sup> with temperatures from 1000 to 16000 K. The plane wave cutoff energy is set to be 600.0 eV. For molecular dynamic simulations, only  $\Gamma$  point of the Brillouin zone is included, while  $4 \times 4 \times 4$  Monkhorst-Pack<sup>26</sup>  $k$  points are used for calculating the electronic structure. Integration of equations of motion proceeds 2000 steps with the time step of 2 fs. Then, the system is equilibrated 200 steps and the final 300 steps are used to calculate physical quantities. During simulations, the ionic temperature  $T_i$  is kept constant at every time step by using velocity scaling. The local thermodynamical equilibrium is reached by setting electron temperature  $T_e$  equal to  $T_i$ . The accuracy of our calculations is examined by the bond length of O<sub>2</sub> molecule in its ground state, and the result is 1.24 Å, which agrees well with the experiment<sup>27</sup>.

### III. PRINCIPAL HUGONIOT AND PAIR CORRELATION FUNCTION

A crucial measurement of the EOS data of oxygen under shock conditions is the Hugoniot<sup>28</sup> which is the locus of points in  $(E, P, V)$ -space satisfying the condition:

$$(E_0 - E_1) + \frac{1}{2}(V_0 - V_1)(P_0 + P_1) = 0, \quad (1)$$

where  $E$  is the internal energy,  $P$  is the pressure,  $V$  is the volume, and the subscripts 0 and 1 denote the initial and shocked state, respectively. This relation follows from conservation of matter, momentum, and energy for an isolated system compressed by a pusher at a constant velocity. In the canonical (NVT) ensemble in which both  $E$  and  $P$  are temperature dependent, the locus of states which satisfy Eq. (1) is the so-called principal Hugoniot, which describes the shock adiabat between the initial and final states. In our first-principles calculations, the internal energy consists of the DFT total energy and the zero-point vibrational energy ( $\frac{1}{2}h\nu_{vib}$  per molecule). The pressure is evaluated via the forces provided by VASP. The particle velocity  $u_p$  and shock velocity  $u_s$  can be derived from the other two Rankine-Hugoniot equations<sup>28</sup>  $V_1 = V_0[1 - (u_p/u_s)]$  and  $P_1 - P_0 = \rho_0 u_s u_p$ . In order to calculate the principal Hugoniot point for a given  $V_1$ , a series of simulations are executed for different temperatures  $T$ .  $(E_0 - E_1)$  and  $\frac{1}{2}(V_0 - V_1)(P_0 + P_1)$  are then fitted to polynomial expansion of  $T$ . The principal Hugoniot temperature  $T_1$  and pressure  $P_1$  are then determined by solving Eq. (1).

As the starting point of the principal Hugoniot curve, it is important to determine the initial state  $(E_0, P_0, V_0)$ . Generally, the initial-state internal energy should be calculated under the experimental condition, with  $\rho=1.2$  g/cm<sup>3</sup> and  $T=77$  K. However, this calculation is highly

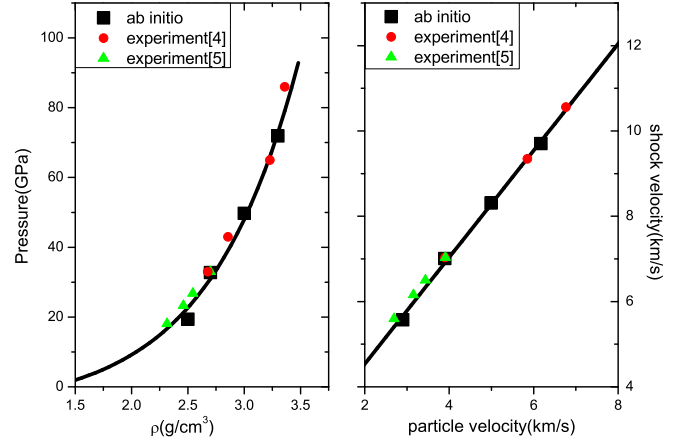


FIG. 1: (Color online). Left panel: Calculated principal Hugoniot curve, in comparison with the previous experimental data; Right panel:  $u_p$ - $u_s$  curve.

TABLE I: Principal Hugoniot points derived from DFT-MD simulation at a series of density ( $\rho$ ), pressure ( $P$ ), and temperature ( $T$ ). The corresponding particle velocity ( $u_p$ ), shock velocity ( $u_s$ ) and dissociation ratio ( $R$ ) are included.

$\rho$ (g/cm <sup>3</sup> )	$P$ (GPa)	$T$ (K)	$u_p$ (km/s)	$u_s$ (km/s)	$R$
2.5	19.4	2413	2.90	5.57	27%
2.7	32.8	5258	3.89	7.01	54%
3.0	49.8	6489	4.99	8.31	69%
3.3	71.9	8823	6.18	9.70	71%

time demanding and is out of our computational capabilities. As an alternative selection, we determine the initial-state energy via single molecule energy. In the present work, we perform PAW potential calculation of an isolated (spin-polarized) O<sub>2</sub> molecule at the equilibrium bond length. With the inclusion of zero point energy, the internal energy  $E_0$  is  $-4.84$  eV/atom at  $T=77$  K. The initial pressure  $P_0$  can be neglected compared with the high pressures of shock compressed states.

The principal Hugoniot curve and  $(u_s, u_p)$  diagram are shown in Fig. 1. We find good agreement between our DFT-MD results and the previous experimental data<sup>4,5</sup>. The present DFT-MD simulations can reasonably reflect the main tendency of oxygen thermodynamic properties along the principal Hugoniot curve. We now investigate explicit nature of the fluid for which the experiments provide only indirect evidence. The probability of finding a atom at distance  $r$  from a reference atom could be given by pair correlation function  $g(r)$ , which is obtained by averaging over all particles and simulation steps in equilibrium. The fraction of molecule can be derived by evaluating the coordination number, which could be expressed as follows:

$$K(r) = \frac{N-1}{V} \int_0^r 4\pi r'^2 g(r') dr'. \quad (2)$$

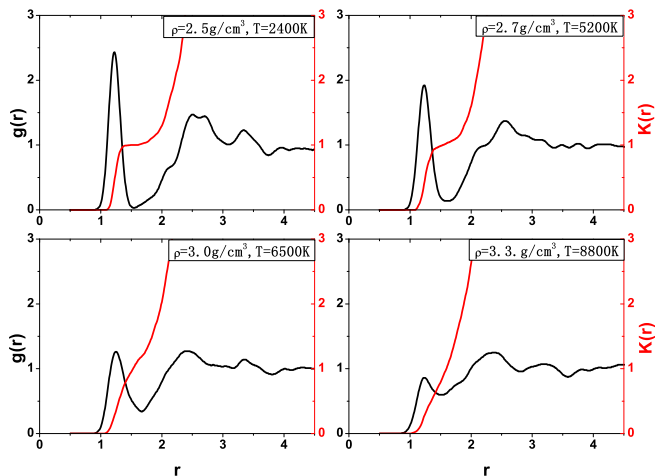


FIG. 2: (Color online). Pair correlation functions (black line) and  $K(r)$  (red line) along the principal Hugoniot curve.

The coordination number is a weighted integral over the pair correlation function  $g(r)$  of the ions.  $N$  is the total number of ions and  $V$  is the volume of the supercell. The value  $K$  at the maximum of  $g(r)$  (around 1.24 Å) is equal to the fraction of molecules in the supercell. The calculated Hugoniot points and related data, such as temperatures and dissociation fraction, are listed in Table I.

Figure 2 shows the pair correlation functions and  $K(r)$  for four densities and temperatures. At the density  $\rho=2.5$  g/cm<sup>3</sup> and  $T=2400$  K, the pair correlation function is featured by a sharp maximum peak around the equilibrium bond length of 1.24 Å, and  $K(1.24) = 73\%$ . Under this condition, the pair correlation function exhibits the typical characteristics of a molecular fluid. As pressure increases, the first main peak begin to reduce in amplitude. This tendency means that the dissociation of O<sub>2</sub> molecules becomes remarkable. The molecule fraction is 46% at  $\rho=2.7$  g/cm<sup>3</sup> and 31% at  $\rho=3.0$  g/cm<sup>3</sup>. The crossover from molecular to atomic fluid exists around  $\rho=2.7 \sim 3.0$  g/cm<sup>3</sup>, and the corresponding principal Hugoniot pressure range from 30 to 50 GPa. Under such conditions, O<sub>2</sub> molecules dissociate gradually.

#### IV. ELECTRONIC STRUCTURE

Metallization of oxygen was first reported by Desgre-niers *et al.*<sup>29</sup> in solid state, with the nonmetal-metal transition accomplished by structural change<sup>30</sup>. The nonmetal-metal transition of oxygen in fluid state was later reported by Bestea *et al.*<sup>6</sup>. The ground state of oxygen is a spin-triplet state under low pressures. The molecular structure and magnetism properties mainly originate from electron spin polarization<sup>31</sup>. Therefore, the electronic structure, which dominates the physical properties, is examined along the principal Hugoniot curve.

Figure 3 shows the isosurfaces of spin densities of oxy-

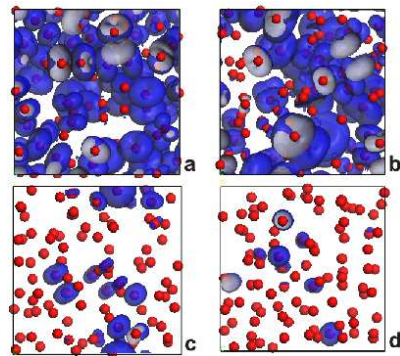


FIG. 3: (Color online). Isosurface of spin density for (a)  $\rho=2.5$  g/cm<sup>3</sup>,  $T=2400$  K, (b)  $\rho=2.7$  g/cm<sup>3</sup>,  $T=5200$  K, (c)  $\rho=3.0$  g/cm<sup>3</sup>,  $T=6500$  K, and (d)  $\rho=3.3$  g/cm<sup>3</sup>,  $T=8800$  K.

gen at the four principal Hugoniot points. At low pressures ( $P = 20 \sim 30$  GPa), the fluid mainly consists of disordered O<sub>2</sub> molecules, and less than 50% fraction of molecules dissociate. In this case, the finite spin polarization characteristic of molecular oxygen is obvious, as shown in Fig. 3(a). As a result, the structural, electrical, and optical properties of the system is closely related with the electron spin polarization of oxygen molecules at low pressures. With the increase of pressures ( $P = 50 \sim 70$  GPa), electron spin polarization is suppressed, and the spin density in the supercell tends to disappear, as shown in Figs. 3(c) and 3(d). This change will consequently affect DOS of the system, which plays a key role in elucidating nonmetal-metal transition and optical properties. As shown in Fig. 4, which plots spin-resolved DOS of shocked oxygen in different pressure regions, a large band gap exists in the DOS when the pressure is about 20 GPa ( $\rho=2.5$  g/cm<sup>3</sup>,  $T=2400$  K), and the system stays in the insulating state. With the increase of pressure, the electrons tend to be delocalized by the non-zero value of DOS at the Fermi energy. Finally, the localized molecular bonds as well as the valence-conduction band gap prominently disappear and the metallic like conductivity emerges at this stage. The nonmetal-metal transition, which is attributed to the dissociation of molecules and thermal broadening of the electronic states, occurs at the pressure range from 30 to 50 GPa. This result agrees well with the experiment<sup>5</sup>.

#### V. OPTICAL PROPERTIES

Having shown the EOS data and nonmetal-metal transition along the principal Hugoniot curve, we turn now to study the optical properties of warm dense oxygen. The frequency dependent dielectric function  $\epsilon(\omega)$  has both real and imaginary parts:

$$\epsilon(\omega) = \epsilon^{(1)}(\omega) + \epsilon^{(2)}(\omega)i. \quad (3)$$

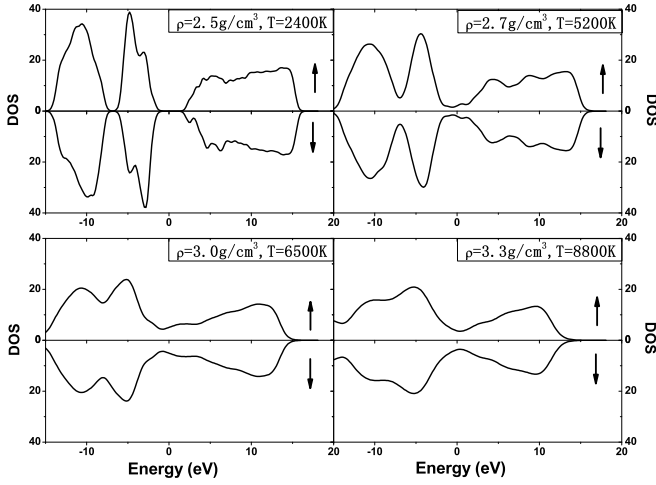


FIG. 4: Spin-resolved electron densities of states along the principal Hugoniot curve. The Fermi energy is set to be zero. (a)  $\rho=2.5\text{ g/cm}^3$ ,  $T=2400\text{ K}$ ; (b)  $\rho=2.7\text{ g/cm}^3$ ,  $T=5200\text{ K}$ ; (c)  $\rho=3.0\text{ g/cm}^3$ ,  $T=6500\text{ K}$ ; (d)  $\rho=3.3\text{ g/cm}^3$ ,  $T=8800\text{ K}$ .

The real  $n(\omega)$  and imaginary  $k(\omega)$  parts of the refraction index are related to the dielectric function by

$$\epsilon(\omega) = \epsilon^{(1)}(\omega) + \epsilon^{(2)}(\omega)i = [n(\omega) + k(\omega)i]^2, \quad (4)$$

or equivalently

$$n(\omega) = \sqrt{\frac{1}{2}[\epsilon(\omega) + \epsilon^{(1)}(\omega)]}, \quad (5)$$

$$k(\omega) = \sqrt{\frac{1}{2}[\epsilon(\omega) - \epsilon^{(1)}(\omega)]}. \quad (6)$$

From the refraction index, the reflectivity  $r(\omega)$  is given by

$$r(\omega) = \frac{[1 - n(\omega)]^2 + k(\omega)^2}{[1 + n(\omega)]^2 + k(\omega)^2}. \quad (7)$$

In Fig. 5 (left panel), we show the variation of the reflectivity  $r(\omega)$  along the principal Hugoniot curve. At lower pressures, for example  $P=20\sim30\text{ GPa}$ , there are two peaks around the photon energies of 5.0 and 11.0 eV, corresponding to the wavelength of 250 and 110 nm, respectively. With the increase in pressure, the peaks vanish. The reflectivity reaches a constant value of 0.172 for the photon energy higher than 35.0 eV. We select a

typical wavelength of 414 nm to investigate the change in reflectivity, as shown in the right panel of Fig. 5. One can see that the reflectivity increases from 0.01 to 0.2 along the principal Hugoniot. The rapid increase in reflectivity occurs at the pressure range from 30 to 50 GPa, with about 50% dissociation of molecules.

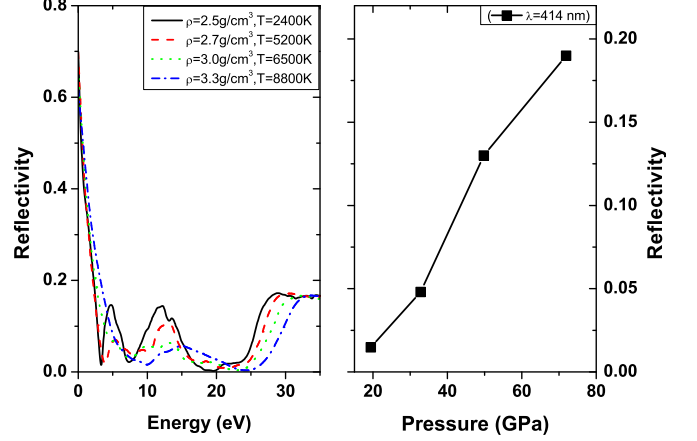


FIG. 5: (Color online) Variation of the frequency-dependent optical reflectivity along the principal Hugoniot (left panel); Reflectivity at a fixed wavelength of 414 nm (right panel).

## VI. CONCLUSION

In summary, we have applied QMD simulations in the study of shock-compressed oxygen. The principal Hugoniot curve has been derived from the computational EOS data, which is consistent well with the experimental measurement. The electron spin polarization, determines physical properties of oxygen at lower pressures, has been shown to be greatly suppressed at higher pressures. This fact, as well as the nonmetal-metal transition and change in reflectivity found in this paper, are attributed to the dissociation of  $\text{O}_2$  molecules. We have determined that the molecular-atomic fluid transition exists at the pressure around 30~50 GPa, which also accord well with the recent experiment.

## Acknowledgments

This work was supported by the Foundation for Development of Science and Technology of China Academy of Engineering Physics under Grant No. 2009B0301037.

\* Corresponding author. zhang\_ping@iapcm.ac.cn

<sup>1</sup> R. J. Hemley, Annu. Rev. Phys. Chem. **51**, 763 (2000).

<sup>2</sup> W. J. Nellis, A. C. Mitchell, M. van Thiel, G.J. Devine, and R. J. Trainor, J. Chem. Phys. **79**, 1480 (1983).

<sup>3</sup> M. D. Knudson, D. L. Hanson, J. E. Bailey, C. A. Hall, J. R. Asay, and C. Deeney, Phys. Rev. B **69**, 144209 (2004).

<sup>4</sup> W. J. Nellis and A. C. Mitchell, J. Chem. Phys. **73**, 6137 (1980).

- <sup>5</sup> D. C. Hamilton, W. J. Nellis, A. C. Mitchell, F. H. Ree, and M. van Thiel, *J. Chem. Phys.* **88**, 5042 (1988).
- <sup>6</sup> M. Bastea, C. Mitchell, and W. J. Nellis, *Phys. Rev. Lett.* **86**, 3108 (2001).
- <sup>7</sup> P. P. Edwards and F. Hensel, *Chem. Phys. Chem.* **3**, 53 (2002).
- <sup>8</sup> C. Mailhot, L. H. Yang, and A. K. McMahan, *Phys. Rev. B* **46**, 14419 (1992).
- <sup>9</sup> A. F. Goncharov, E. Gregoryanz, H. k. Mao, Z. X. Liu, and R. J. Hemley, *Phys. Rev. Lett.* **85**, 1262 (2000).
- <sup>10</sup> A. S. Balchan and H. S. Drickamer, *J. Chem. Phys.* **34**, 1948 (1961).
- <sup>11</sup> R. Reichlin, K. M. Andrew, R. Marvin, and M. Sue, *Phys. Rev. B* **49**, 3725 (1994).
- <sup>12</sup> B. Militzer, F. Gygi, and G. Galli, *Phys. Rev. Lett.* **91**, 265503 (2003).
- <sup>13</sup> J. D. Kress, S. Mazevet, L. A. Collins, and W. W. Wood, *Phys. Rev. B* **63**, 024203 (2000).
- <sup>14</sup> B. Militzer, *Phys. Rev. B* **79**, 155105 (2009).
- <sup>15</sup> M. Ross and F. H. Ree, *J. Chem. Phys.* **73**, 6146 (1980).
- <sup>16</sup> Q. F. Chen, L. C. Cai, Y. Zhang, and Y. J. Gu, *J. Chem. Phys.* **128**, 104512 (2008).
- <sup>17</sup> T. R. Mattsson and M. P. Desjarlais, *Phys. Rev. Lett.* **97**, 017801 (2006).
- <sup>18</sup> A. Kietzmann, B. Holst, R. Redmer, M. P. Desjarlais, and T. R. Mattsson, *Phys. Rev. Lett.* **98**, 190602 (2007).
- <sup>19</sup> G. Kresse and J. Hafner, *Phys. Rev. B* **47**, R558 (1993).
- <sup>20</sup> G. Kresse and J. Furthmüller, *Phys. Rev. B* **54**, 11169 (1996).
- <sup>21</sup> T. Lenosky, S. Bickham, J. Kress, and L. Collins, *Phys. Rev. B* **61**, 1 (2000).
- <sup>22</sup> S. Bagnier, P. Blottiau, and J. Clerouin, *Phys. Rev. E* **63**, 015301(R) (2001).
- <sup>23</sup> P. E. Blöchl, *Phys. Rev. B* **50**, 17953 (1994).
- <sup>24</sup> G. Kresse and D. Joubert, *Phys. Rev. B* **59**, 1758 (1999).
- <sup>25</sup> J. P. Perdew, *Electronic Structure of Solids* (Akademie Verlag, Berlin, 1991).
- <sup>26</sup> H. J. Monkhorst and J. D. Pack, *Phys. Rev. B* **13**, 5188 (1976).
- <sup>27</sup> K. P. Huber and G. Herzberg, *Molecular Spectra and Molecular Structure. IV. Constants of Diatomic Molecules* (Van Nostrand-Reinhold, New York, 1979).
- <sup>28</sup> Y. Zeldovich and Y. Raizer, *Physics of Shock Wave and High Temperature Hydrodynamic Phenomena* (Academic Press, New York, 1966).
- <sup>29</sup> S. Desgreniers, Y. K. Vohra, and A. L. Ruoff, *J. Phys. Chem.* **94**, 1117 (1990).
- <sup>30</sup> G. Weck, P. Loubeyre, and R. LeToullec, *Phys. Rev. Lett.* **88**, 035504 (2002).
- <sup>31</sup> K. Sugimori, T. Oda, H. Nagao, I. Hamada, S. Kagayama, M. Geshi, H. Nagara, K. Kusakabe, and N. Suzuki, *J. Phys.: Condens. Matter* **19**, 365211 (2007).